ESRF

EUROPEAN SYNCHROTRON RADIATION FACILITY

INSTALLATION EUROPEENNE DE RAYONNEMENT SYNCHROTRON

Experiment Report Form

The double page inside this form is to be filled in by all users or groups of users who have had access to beam time for measurements at the ESRF.

Once completed, the report should be submitted electronically to the User Office via the User Portal:
https://wwws.esrf.fr/misapps/SMISWebClient/protected/welcome.do

Deadlines for submission of Experimental Reports

Experimental reports must be submitted within the period of 3 months after the end of the experiment.

Experiment Report supporting a new proposal ("relevant report")

If you are submitting a proposal for a new project, or to continue a project for which you have previously been allocated beam time, you must submit a report on each of your previous measurement(s):

- even on those carried out close to the proposal submission deadline (it can be a *"preliminary report"),*
- even for experiments whose scientific area is different form the scientific area of the new proposal,
- carried out on CRG beamlines.

You must then register the report(s) as "relevant report(s)" in the new application form for beam time.

Deadlines for submitting a report supporting a new proposal

- 1st March Proposal Round - **5th March**
- 10th September Proposal Round - **13th September**

The Review Committees reserve the right to reject new proposals from groups who have not reported on the use of beam time allocated previously.

Reports on experiments relating to long term projects

Proposers awarded beam time for a long term project are required to submit an interim report at the end of each year, irrespective of the number of shifts of beam time they have used.

Published papers

All users must give proper credit to ESRF staff members and proper mention to ESRF facilities which were essential for the results described in any ensuing publication. Further, they are obliged to send to the Joint ESRF/ ILL library the complete reference and the abstract of all papers appearing in print, and resulting from the use of the ESRF.

Should you wish to make more general comments on the experiment, please note them on the User Evaluation Form, and send both the Report and the Evaluation Form to the User Office.

Instructions for preparing your Report

- fill in a separate form for each project or series of measurements.

- type your report in English.
- include the experiment number to which the report refers.
- make sure that the text, tables and figures fit into the space available.
- if your work is published or is in press, you may prefer to paste in the abstract, and add full reference details. If the abstract is in a language other than English, please include an English translation.

	Experiment title: Lateral organisation of plasma membrane lipids: effect of oxidative stress	**Experiment number**: SC-4816
Beamline: ID10	**Date of experiment**: from: 13/6/18 to: 19/6/18	**Date of report**: 01/07/19
Shifts: 18	**Local contact(s)**: Andrei Chumakov (Oleg Konovalov)	*Received at ESRF:*

Names and affiliations of applicants (* indicates experimentalists):

Bob-Dan Lechner*, C. Peter Winlove, Peter G. Petrov*

University of Exeter, Stocker Road, EX44QL, Exeter, UK

Report:

1. Experiment details

Experiments were performed using the purpose-built Langmuir trough on the liquid diffractometer at the TROIKA II beamline ID10b. The monolayers were spread at the air/water interface and examined at different states of compression. Four model monolayers were tested on different subphases (varying ionic strength and pH) comprising the following lipid species (in varying proportions): 1,2-dipalmitoyl-sn-glycero-3-phosphocholine (DPPC), 1,2-dipalmitoyl-sn-glycero-3-phosphoethanolamine (DPPE), 1,2-dipalmitoyl-sn-glycero-3-phospho-L-serine (DPPS), N-palmitoyl-D-erythro-sphingosylphosphorylcholine (SM) and cholesterol (chol), akin to the two leaflets of the red blood cell (RBC) lipid membrane:

1. Outer leaflet (OL): DPPC : DPPE : DPPS : Cholesterol : SM (31 : 9 : 1 : 20 : 39 wt%)
2. Inner leaflet (IL): DPPC : DPPE : DPPS : Cholesterol : SM (12 : 38 : 22 : 20 : 8 wt%)
3. Inner leaflet (as 2.) but excluding cholesterol to investigate the role of cholesterol in the lateral ordering of the IL.
4. Inner leaflet (as 2.) but containing 7-ketocholesterol instead of cholesterol to mimic a monolayer under oxidative stress. 7-ketocholesterol is one of the main products of cholesterol oxidation in RBCs.

Furthermore, the individual components (DPPC, DPPE, DPPS) of the complex RBC-like monolayer mixtures were measured.

Scattering was collected using monochromatic X-rays (C (111) crystal channel cut monochromator) and the two-component detector arm. The micro-beam setup was used featuring a beam size of 100 × 300 μm^2 at an energy of 8 keV, 200 mA (λ = 1.55 Å) with a high photon flux of 2.7×10^{12} ph/s. The double crystal deflector allowed to perform XRR experiments from the liquid surface without moving the sample. To collect reflected intensity, the P100K detector was used. In GIXD experiments, the monolayer is illuminated at an angle of incidence of α_i = 0.1233°, slightly below the critical angle for total reflection of α_{cr} = 0.154° and so the lateral organization of the acyl chains and cholesterol was studied with the Mythen 1K detector.

3. Results

The experiments carried out at beamline ID10b gave important structural information in addition to our previous investigations of the same systems using fluorescence microscopy, surface relaxation techniques and Molecular Dynamics simulations, in which we established that the IL and OL monolayers are rigid and probably contain highly organized domains with densely packed lipid acyl chains over a wide range of lateral pressures.

We acquired XRR curves for all four monolayers at different surface pressures (π) that exhibited an increasing degree of order in the *z*-direction with increasing π. At 30 mNm^{-1}, we observed fairly similar reflectivity scans (Fig.1, left) for the three different IL-like and the OL-like monolayers on a buffer solution containing mono- (Na^+) and divalent cations (Ca^{2+}). The XRR curves can be extrapolated using the slab model of electron density. Electron density distributions across the monolayer were calculated (Fig.1, middle) and it can be seen that the composition has a major influence on the electron density profile. While the total monolayer thickness remains roughly the same for all RBC-like monolayers, the distribution between headgroup and acyl chain thickness varies (Fig.1, right). The OL monolayer shows a much thicker headgroup and smaller acyl chains as compared to the IL monolayer. This might be due to the higher content of lipids with intrinsically large headgroups like PC and SM in the OL monolayer. The acyl chain thickness might be decreased in this case due to a tilt of the crystallized acyl chains relative to the interface normal, which is a usual scenario for pure PC monolayers, or somewhat less ordered acyl chains. However, the very complicated mixture of 5 component does not allow to answer this question easily. On the other hand, the main lipid species in the IL mixture are PE and PS with comparatively small headgroups, hence the smaller average headgroup size in the IL mixture and the sharper and somewhat higher maximum at the phosphate group region of the electron density. The IL monolayer and the IL monolayer without cholesterol show very similar head group and acyl chain thicknesses. The presence or absence of cholesterol seems to change these thickness distributions only slightly. The oxidation of cholesterol, however, has a drastic impact on the thickness ratio. For the IL 7KetoChol monolayer, the headgroup slab is increased significantly in size in comparison to the IL monolayer with normal cholesterol, and the headgroup slab is even thicker than for the OL monolayer that features lipids with larger headgroups. The oxidized 7-Ketocholesterol is more hydrophilic and thus prefers to be closer to the phospholipid's headgroup region, increasing their effective size. Molecular Dynamics simulations also show that more water molecules seem to be drawn deeper into the monolayer as compared to the IL monolayer with normal cholesterol. Those 2 effects lead to an increase of the size of the hydrophilic headgroup region and seems to cause a disordering of the acyl chains and hence the decrease in acyl chain layer thickness and somewhat flattening of the electron density profile in the phosphate group region. The oxidised cholesterol, 7-Ketocholesterol, obviously has a major impact on lipid order and monolayer structure.

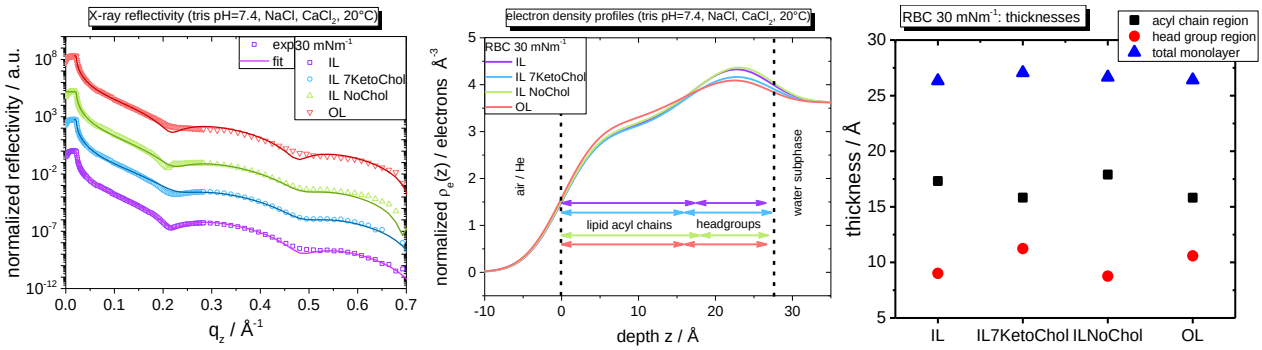

Figure 1. XRR behaviour of RBC-like monolayers. Left: XRR curves for RBC IL (purple), IL 7-KetoChol (blue), IL NoChol (green) and OL (red) monolayers on tris buffer (pH=7.4, 150 mM NaCl, 50 mM $CaCl_2$) at 20°C, experimental data (symbols) and simulated data (lines). Middle: electron density profiles calculated from the XRR curves with the same colour code. Right: Plot of the thickness of the head group (red circles), the acyl chain (black squares) and the whole monolayer (blue triangles) for all 4 investigated RBC-like monolayers.

We acquired 2D GIXD patterns for all the monolayers, which we integrated over q_z to obtain 1D Bragg peak (Fig. 2, left) and compare them to each other. At 30 mNm^{-1}, the 1D diffraction curve for all 3 IL monolayer show a single Bragg peak at 1.499 Å^{-1} (Fig. 2, left), indicating the presence of a hexagonal lattice. Thereby, the diffracted intensity is the highest for the monolayer without cholesterol and the IL monolayer with normal cholesterol shows decreased intensity in comparison. Oxidation of cholesterol leads to a further decrease in intensity. The full width half maximum (fwhm) of the diffraction peak is a indicator for the order of the acyl chains and related to the coherence length of the mosaic structure of the crystaline acyl chain layer (L_c = 0.9 ×2π/ fwhm). For the IL monolayer with normal cholesterol, L_c = 177 Å, which is the highest value of the three IL-like films and the acyl chains are ordered into rather large domains of equal crystal orientation. When cholesterol is removed this order is somewhat reduced. Oxidation of cholesterol, however, results in a drastic further reduction of L_c and thus the acyl chain order. This is in accordance with the findings from the XRR experiments and proves that 7-ketocholesterol causes a higher disorder in the alcyl chain region, compared to the IL monolayer with normal or no cholesterol, and hence the reduction in acyl chain layer thickness as found from the electron density curves. The OL monolayer, on the other hand, shows a more complex diffraction pattern, featuring 2 diffration peaks. This possibly indicates the presence of a distorted hexagonal latice featuring the {10} and {1-1} reflexes which are well separated. Due to the high content of PC in the OL monolayer it might be possible that domains of the interfacial film show lipids with tilted acyl chains, resulting in a herring-bone or pseudo-herring-bone lattice. Also, a rectangular acyl chain lattice could lead to the present GID pattern.

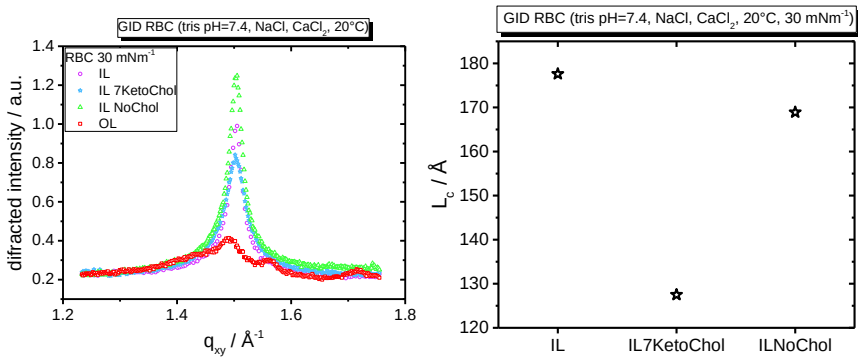

Figure 2. GID behaviour of RBC-like monolayers. Left: Bragg peaks (baseline corrected) in 1D GID curves integrated over q_z for RBC IL (purple circles), IL 7-KetoChol (blue stars), IL NoChol (green triangles) and OL (red squares) on tris buffer (pH=7.4, 150 mM NaCl, 50 mM $CaCl_2$) at 20°C. Right: Coherence lengths calculated from the fwhm of the Bragg peak for all the IL monolayer.

Of the pure lipid monolayers investigated, we would like to point out the DPPS monolay and its response to the ionic strength of the subphase. In Figure 3, reflectivity curves (left) and electron density profiles (right) of DPPS monolayer are compared for measurements on a pure water and on a tris buffer (pH=7.4, 150 mM NaCl, 50 mM $CaCl_2$) subphase, respectively. It is obvious that at 30 mNm^{-1} even the XRR curves are remarkably different depending on the subphase's ionic strength and the electron density profiles also show a very different shape for different subphases. This is the case for the lipid monolayers at 30 mNm^{-1} and also at smaller surface pressueres like 15 or 3 mNm^{-1} (data not shown). DPPS shows a charged headgroup that responds to an ionic subphase by adapting the headgroup order and thus the ordering of the acyl chains can be influenced as well. This is an important factor to be taken into account when discussing or studying the complex RBC-like monolayers, especially the IL-like monolayer that feature a high PS-content. A single peak is visible in the GID data with a maximum at 1.499 Å regardless of the subphase. However, the intensity and fwhm is decreased the case of the ionic subphase, indicating a better ordering of the acyl chains in the DPPS monolayer on the water subphase.

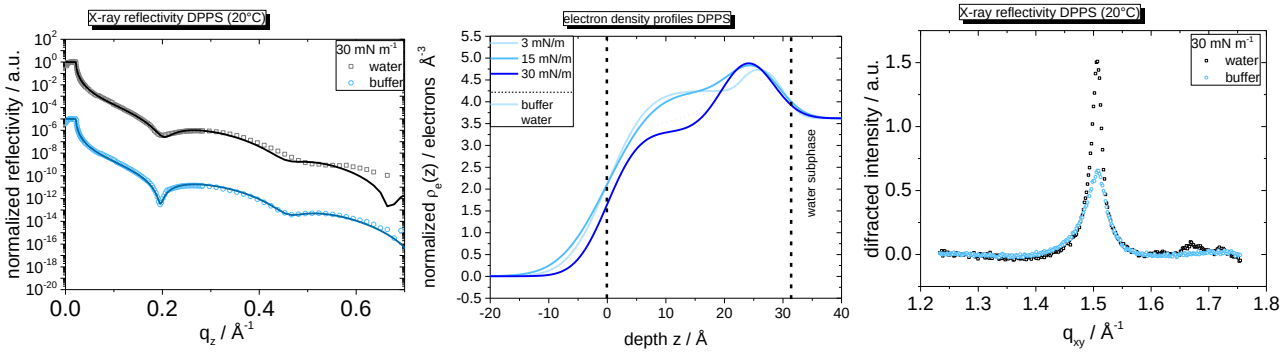

Figure 3. XRR curves (left), electron density plots (middle) and 1D GID data (right) of DPPS monolayers on a water (left/right: black symbols for experimental data and black lines for fitted data; middle: dotted lines) or tris buffer (pH=7.4, 150 mM NaCl, 50 mM $CaCl_2$) subphase (left/right: blue symbols for experimental data and blue lines for fitted data; middle: straight lines) at surface pressueres given in the graph.

4. Conclusions and future work

We demonstrated the feasibility of investigating complex multicomponent monolayers of compositions akin to the individual leaflets of the red blood cell using XRR and GIXD experiments. We established the existence of highly ordered hexagonal or rectangular arrangements in the systems. The information obtained from these experiments will serve to critically examine and quantify phenomenological models of the lateral and 3D structure of RBC monolayers as derived from Molecular Dynamics simulations.

The present study employed model systems with saturated acyl chain to evaluate the effects arising from the headgroup distribution. It will serve as a basis for further experiments of more physiologically relevant systems featuring unsaturated chains or originating from red cell extracts. The established methodology of evaluating the effects arising from oxidative stress could serve to identify disease related oxidation effects on different membrane species. In addition, this work will allow the investigation of the role of environmental parameters such as subphase composition, in order to more closely mimic the native conditions of RBC membranes. We expect these results to lead to better understanding of the changes observed in various red cell-related diseases involving oxidative stress and help inform novel therapeutic strategies.